Uncertainties in Aspheric Profile Measurements with the Geometry Measuring Machine at NIST

Ulf Griesmann[a], Nadia Machkour–Deshayes[a], Johannes Soons[a], Byoung Chang Kim[a], Quandou Wang[a], John R. Stoup[a], and Lahsen Assoufid[b]

[a]National Institute of Standards and Technology (NIST), Manufacturing Engineering Laboratory, Gaithersburg, MD 20899-8223, U.S.A.

[b]Advanced Photon Source (APS), Argonne National Laboratory, Argonne, IL 60439, U.S.A.

ABSTRACT

The Geometry Measuring Machine (GEMM) of the National Institute of Standards and Technology (NIST) is a profilometer for free-form surfaces. A profile is reconstructed from the local curvature of a test part surface, measured at several locations along a line. For profile measurements of free-form surfaces, methods based on local part curvature sensing have strong appeal. Unlike full-aperture interferometry they do not require customized null optics. The uncertainty of a reconstructed profile is critically dependent upon the uncertainty of the curvature measurement and, to a lesser extent, on curvature sensor positioning accuracy. For an instrument of the GEMM type, we evaluate the measurement uncertainties for a curvature sensor based on a small aperture interferometer and then estimate the uncertainty that can be achieved in the reconstructed profile. In addition, profile measurements of a free-form mirror using GEMM are compared with measurements using a long-trace profiler, a coordinate measuring machine, and subaperture-stitching interferometry.

Keywords: Profilometer, surface curvature, aspheric surface profile

1. INTRODUCTION

Full-aperture interferometry has evolved into a general test method in the production of flat and spherical precision surfaces. Modern interferometers use electronic imaging systems which can provide near instantaneous form error information for entire surfaces. Typically interferometers can be used to measure a wide range of flat and spherical surfaces. The difficulty in using interferometry for testing aspheric surfaces is widely acknowledged. Apart from certain quadric surfaces, for which special test setups can be used, aspheric surfaces and wavefronts must be tested using "null optics". Null optics are precision optics that are not only expensive, but also create additional metrology problems. This situation has led to many attempts to develop alternative metrology methods in order to lower the cost of measuring aspheric surfaces.

One idea that has been pursued repeatedly is to base the measurement of a profile, or a surface, on measurements of the curvature. From a geometric point of view this approach has considerable appeal. Interferometers, and coordinate measuring machines, are used to measure a profile, or surface, of a part relative to an absolute external reference. In the case of interferometers, this is a flat or spherical reference wavefront which is usually created using an appropriate reference surface. In a coordinate measuring machine the coordinate reference is embodied in the straightness of its guideways, their alignment, and the accuracy of its scales. A measurement made with these methods provides information on the form of the part together with information on its orientation, or alignment, with respect to the external reference. In interferometry of aspheric surfaces, it can be difficult to separate form information from alignment information. In a profilometer based on curvature sensing, the measurands are intrinsic parameters of a profile, or surface, which completely determine the form[1] regardless of the orientation and position relative to an external reference.

We will restrict ourselves to the measurement of one-dimensional surface profiles $z(y)$ in a plane where z is the profile "height" and y the position. In Cartesian coordinates, the following non-linear differential equation[2] relates the profile $z(y)$ to the curvature $k(y)$ at each point:

$$\frac{d^2z(y)}{dy^2} = k(y) \cdot \left[1 + \left(\frac{dz(y)}{dy}\right)^2\right]^{\frac{3}{2}} . \tag{1}$$

Author e-mail information: ulf.griesmann@nist.gov

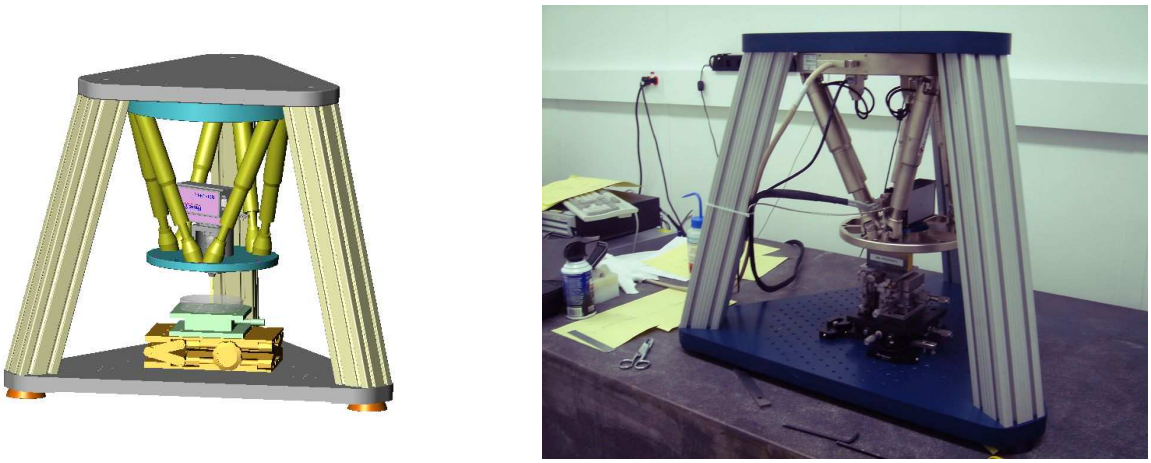

Figure 1. Solid model of NIST's prototype Geometry Measuring Machine (GEMM) on the left and photograph of the actual instrument (right).

This is a form of the Frenet equations which describe arbitrary curves in space.[1] Eq. 1 may be interpreted in two ways: either given a profile $z(y)$, the curvature of a profile at any point can be calculated, or, when the curvature $k(y)$is known, it can be used to reconstruct the profile $z(y)$ by integration.

The first to apply these geometric concepts to the problem of profiling aspheric surfaces was Glenn.[3,4] His ideas were later refined when the Physikalisch-Technische Bundesanstalt (PTB), Germany, proposed the Large Area Curvature Sensor (LACS) instrument for profiling steep aspheric surfaces.[5–13] The Geometry Measuring Machine (GEMM) of the National Institute of Standards and Technology (NIST) is a prototype instrument for profiling precision aspheric surfaces based on curvature sensing. GEMM is built from commercially available parts and, like LACS, uses a small interferometer as its curvature sensor. The purpose of GEMM is to evaluate profile and surface metrology based on curvature sensing, to determine the uncertainty that can be achieved in profile- and surface- measurements, and to find out if curvature sensing profile- and surface- metrology will be able to compete with established metrology methods such as interferometry.

2. THE GEOMETRY MEASURING MACHINE (GEMM) AT NIST

The mechanical design of the GEMM prototype at NIST is shown in Fig. 1. For clarity, a solid model of GEMM is shown together with a photograph of the actual instrument. A simple machine frame was created from two aluminum plates which are connected by three sturdy aluminum pillars. GEMM uses a compact phase-measuring Twyman-Green interferometer for the measurement of the local curvature at many points along a line on the part surface under test. GEMM needs a curvature sensor with a very low measurement uncertainty. We chose an interferometer as the curvature sensor in GEMM, primarily because a suitable compact phase-measuring interferometer was commercially available. Disadvantages of using a phase-measuring interferometer as the curvature sensor are the limited dynamic range, and the high degree of redundancy in the acquired data, which requires a whole image to be acquired for a single curvature value.[14] In a prototype instrument these are only minor concerns, but it may be necessary to evaluate alternative means for curvature sensing with improved efficiency in a production instrument. The test beam of the interferometer is collimated and beam diameters of 2 mm and 10 mm can be selected by changing objective lenses. During a profile measurement the interferometer must be moved from one grid point to the next and it must be possible to adjust the tilt of the interferometer so that the test beam is nearly normal to the surface, which requires an accurate motion control system. For surface scans, at least 5 degrees of freedom are required. In GEMM, a Stewart platform, or Hexapod robot, is used to move the interferometer. The Stewart platform in GEMM is a stiff, stable motion system with 6 degrees of freedom which has a standard position uncertainty of 1 μm for the translational degrees of freedom. A computer controls both the phase-measuring interferometer and the Stewart platform. They are integrated with the MATLAB† environment, which is used as a flexible means to script all measurement procedures. GEMM is installed in a temperature-controlled laboratory on a vibration-isolated granite table.

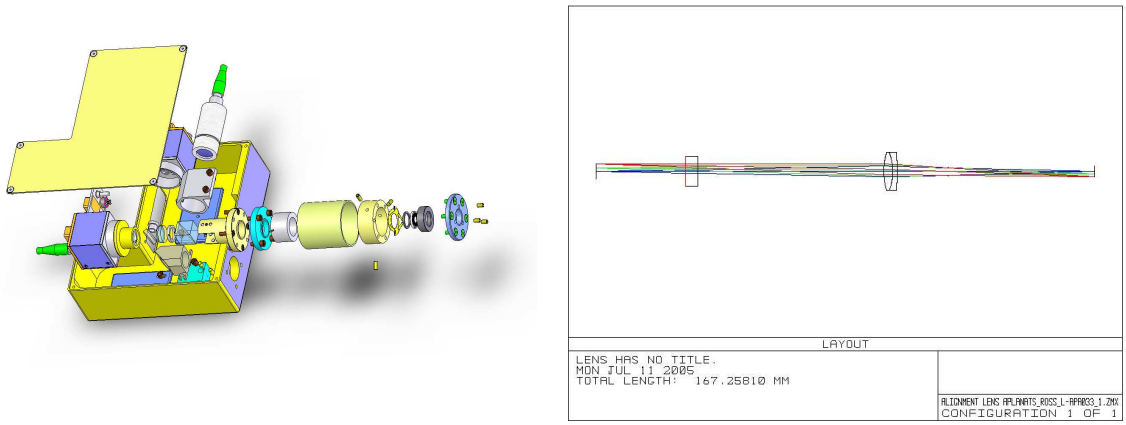

Figure 2. Solid model of the Small Aperture Digital Interferometer (SADI) developed at NIST (left) and ray-trace model of the imaging system (right). SADI is a Fizeau interferometer with collimated test beam of 5 mm diameter. The dimensions of the interferometer are approximately 10 cm $\times$ 10 cm $\times$ 4 cm. The ray-trace model shows the beam splitter and the imaging system which consists of a single lens.

2.1. A Future GEMM Curvature Sensor

In section 3.2, we discuss the need for the GEMM curvature sensor to measure not only the local shape of a surface, but also the distance of the sensor to the surface. A new curvature sensor for GEMM is now under construction at NIST, which will be able to make simultaneous form and distance measurements. The new sensor is specifically designed for GEMM and avoids a number of problems that we encountered with the general purpose interferometer currently used as the curvature sensor. The new sensor will be a compact Fizeau interferometer, the "Small Aperture Digital Interferometer" (SADI). A solid model of the interferometer can be seen in Fig. 2. SADI has a collimated test beam of 5 mm diameter. The dimensions of the interferometer are approximately 10 cm $\times$ 10 cm $\times$ 4 cm. The optical model of the interferometer is shown in Fig. 2 on the right. Every interferometer design is a compromise between the need to observe clean interference fringes, which carry the surface height information, and good imaging of the surface under test, which makes it possible to relate the height measurement to test part coordinates. An undistorted image often requires a large number of optical surfaces, creating coherent stray light and "ghost fringes" in the interferometer, which reduces the accuracy of height measurements. SADI is designed to achieve a low uncertainty for surface height measurements while permitting some image distortion. The interferometer has a very simple imaging system, consisting of just one lens, to reduce undesirable coherent reflections as much as possible. Because SADI has fixed object and image distances, any residual distortion by the imaging system can be calibrated and corrected numerically after image acquisition. The design wavelength for SADI is 633 nm. The wavelength of the laser can be shifted for phase measuring and to enable measurement of the distance between the reference surface of SADI and the test part surface.

3. COMPUTER SIMULATION OF GEMM MEASUREMENTS

We have undertaken computer simulations to understand the effect of uncertainties in the GEMM measurement procedure and the resulting uncertainty in the profile measurements. The test part for the simulations was an aspheric surface which is described by the following well known equation:

$$z(y) = \frac{y^2}{R}\left(\frac{1}{1+\sqrt{1-(K+1)\frac{y^2}{R^2}}}\right). \tag{2}$$

y is the position coordinate and R is the vertex radius of the surface at $y = 0$. The conic constant K was set to -1.6, which makes the surface a hyperboloid. (This value of the conic constant was chosen because we have a hyperbolic mirror with the same conic constant and a vertex radius of 0.2 m.) In the computer simulation we studied parts with vertex radii, R, of 0.08 m, 0.8 m, 8 m, and 80 m. These cover a range from a relatively small radius up to the large radii that are

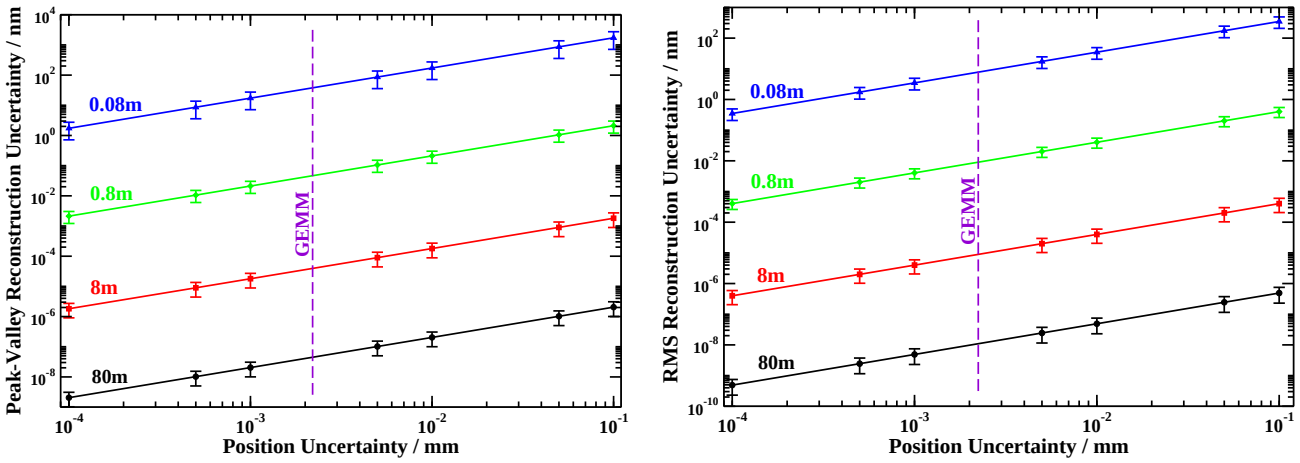

Figure 3. Reconstruction error as function of sensor position uncertainty. The standard position uncertainty of GEMM (2.2 μm) is indicated with a vertical dashed line. Error bars in this and the following figures indicate a range equal to two standard uncertainties.

found in imaging systems for synchrotron radiation beamlines. A part diameter of 86 mm was assumed for all radii. The profile measurements were simulated along the radial direction of all four surfaces. There are two sources of measurement uncertainty inherent in the GEMM method and these are the uncertainty in knowing the position where the part curvature is measured and the uncertainty in the curvature measurement itself. In the following sections, we discuss the magnitude of these uncertainties and their effect on profile reconstruction. Some aspects of the GEMM method that affect only high order terms of the reconstructed profiles are not discussed here. Among these are the influence of size of the test beam diameter and the spacing between the curvature measurements along a profile.

3.1. Effect of Uncertainty in Sensor Positioning

An error in positioning the curvature sensor along the profile leads to a second-order error in the curvature measurement. The profile reconstruction uncertainty that is affected by sensor position uncertainty is a consequence of the aspheric departure of the surface from a sphere. For the profile of a sphere, a position error is without consequence because the curvature does not depend on the measurement position. Larger departures of the aspheric surface from the best-fit sphere are expected to lead to larger profile reconstruction uncertainties. The profile reconstruction was simulated for parts with different vertex radii, R, in Eq. 2. Fig. 3 shows the peak-to-valley reconstruction error (left) and the rms reconstruction error (right) for the different radii. In calculating the graphs of Fig. 3 we assume that the position errors of our Stewart platform are normally distributed about the nominal positions. The abscissæ of the graphs are the standard deviations of the distribution of position errors. At every point shown in Fig. 3, a GEMM measurement, subject to the position error of the stage, was simulated 20 times. The procedure described by Elster et al.[15] was used to integrate Eq. 1 with the simulated curvature measurements. Because the analytical form of the profile is known in the simulation (Eq. 2) we can use Eq. 1 to calculate the curvature at any given position. The reconstruction error, which is the deviation of the reconstructed profile from the ideal profile (Eq. 2), was calculated in both the peak-to-valley and rms sense. Fig. 3 shows the means of the 20 values for the reconstruction error; the standard deviation of the reconstruction errors is indicated with error bars.

The position uncertainty is the lack of knowledge of the true measurement location of the GEMM sensor on the test part surface. This depends both on the positioning uncertainty of the motion control system and, because pointing errors of the sensor translate into position errors, on the angular uncertainty. For the three linear degrees of freedom of the Stewart platform, the standard positioning uncertainty is 1 μm. The angular uncertainty of the Stewart platform is specified by the supplier as 20 μrad. The distance between part surface and the point at which the interferometer is mounted to the Stewart platform is about 3 cm for the 10 mm objective of the interferometer, and 10 cm for the 2 mm objective. In the worst case, the 2 mm objective, the pointing uncertainty of the interferometer leads to an uncertainty of the measurement location of 2 μm. When the two contributors to the position uncertainty are added in quadrature, a standard uncertainty for the measurement position of 2.2 μm results.

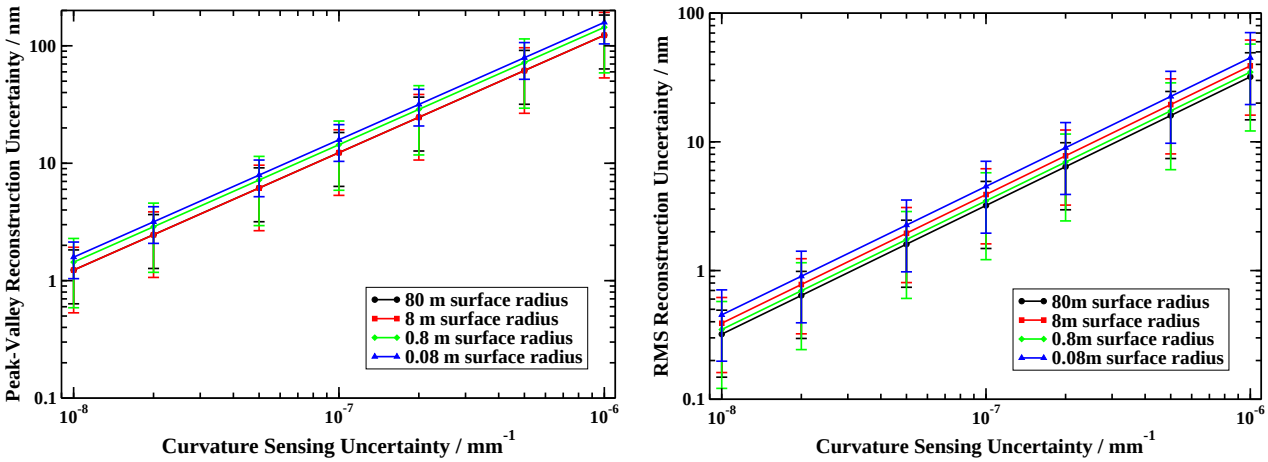

Figure 4. Reconstruction uncertainty as function of curvature sensing uncertainty.

Fig. 3 shows that the reconstruction uncertainty for the aspheric profiles is strongly dependent on the vertex radius of the surface. This is expected because the change in curvature is lower for a surface with larger radius and a position error will result in a smaller error in the curvature measurement. For part radii larger than about 0.2 m the reconstruction error drops below 1 nm for the position uncertainty of the GEMM motion control system. For even larger part radii the position error of the motion control system is of no consequence. A position uncertainty in the vicinity of 1 μm can be accomplished with relatively modest motion control systems, such as the Stewart platform of GEMM, which do not require laser interferometers. Measurements of surfaces with larger aspheric departure from the spherical form will have greater sensitivity to position errors.

3.2. Effect of Uncertainty in Curvature Sensing

The uncertainty in curvature sensing has a direct effect on the uncertainty of the profile reconstruction. Two types of curvature sensing uncertainty must be considered. The curvature sensor may be biased, which will lead to an error in the reconstructed profile. Any bias must be removed by calibrating the sensor, which is discussed in section 3.3. Here we deal with non-repeatable errors in the curvature sensing. We assume again that the curvature values measured by the sensor are normally distributed about a mean. In Fig. 4 we show the reconstruction uncertainty that follows from the uncertainty in the curvature sensing of our four surfaces with vertex radii ranging from 0.08 m to 80 m. It is clear from Fig. 4 that curvature sensing uncertainties lower than $10^{-7}\,\mathrm{mm}^{-1}$ must be achieved for profile reconstruction uncertainties in the vicinity of 1 nm, and this is independent of the surface radius.

The two main contributors to the uncertainty of curvature measurements are illustrated in Fig. 5. The graphs show curvature measurements, made with GEMM, for mirrors with 0.2 m, 2 m, and 84 m radius. Because the curvature of the reflected wavefront exceeds the dynamic range of the interferometer with the 10 mm objective, the mirrors with 2 m and 84 m radius were measured with the 10 mm diameter test beam and the 0.2 m radius mirror was measured with the 2 mm diameter test beam of the GEMM interferometer. For all three mirrors, measurements were made at different distances of the sensor to the mirror surface. The measurements were repeated 10 times to determine the repeatability. For the mirror with the 84 m radius, the change in curvature of the test wave with sensor distance is so small that it cannot be detected. For the mirrors with smaller radii, the curvature measurement depends noticeably on the distance between the sensor and the mirror surface. It follows that this distance must be well-controlled in GEMM to obtain a sufficiently low uncertainty for the curvature measurement. The results for all mirrors are summarized in Table 1. The value for the reproducibility u_k in the table is the average of the reproducibilities for all z-positions. u_k is low enough to permit a profile reconstruction uncertainty below 10 nm for the 10 mm diameter test beam, but considerably larger for the 2 mm test beam. The reason is the 2 mm objective, which has many optical surfaces and produces an interferogram with more edge diffraction and stray light effects, and these directly affect the measurement repeatability. In the case of the 2 mm test beam, the response of curvature to sensor displacement is also non-linear at the ends of the range. In the last column of Table 1, we calculate the uncertainty in distance between part and sensor which would result in a curvature uncertainty of $10^{-8}\,\mathrm{mm}^{-1}$. For the

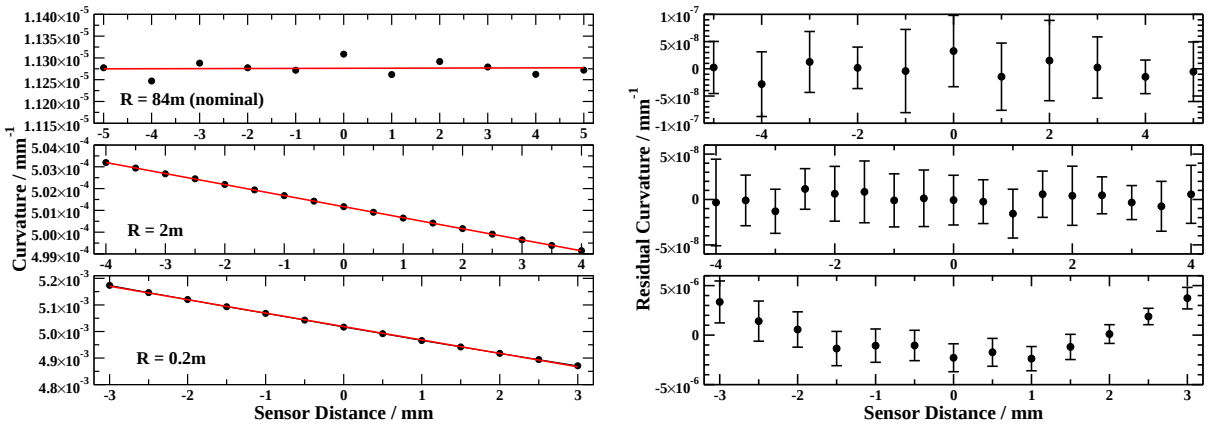

Figure 5. Measured curvature as function of sensor distance to part surface for surface radii of 0.2 m, 2 m, and 84 m (left). The abscissæ are the distance relative to the nominal object distance of the objective. The best fi t line through the data is indicated. The same data are shown on the right with the best fi t line subtracted to clearly show residua and standard uncertainties.

Mirror Radius [m]	Test beam diameter [mm]	Slope $\frac{dk}{dz}$ [mm^{-2}]	$u_k(z)$ [mm^{-1}]	δz [mm]
84	10	$2.4{\cdot}10^{-10}$	$5.64{\cdot}10^{-8}$	42
2	10	$-5{\cdot}10^{-7}$	$2.84{\cdot}10^{-8}$	$2{\cdot}10^{-2}$
0.2	2	$-5.05{\cdot}10^{-5}$	$1.5{\cdot}10^{-6}$	$2{\cdot}10^{-4}$

Table 1. Sensitivity of curvature measurement to sensor distance between test part surface and sensor for three different mirrors. u_k is the repeatability of curvature measurements, and δz the uncertainty in sensor to surface distance that is required to achieve a curvature uncertainty of 10^{-8} mm^{-1}.

mirror with the smallest radius, the permissible uncertainty for the distance between part surface and sensor is 200 nm, which is easily realized with an interferometric distance sensing method.

3.3. Effect of Curvature Sensor Bias and Calibration

Any curvature sensor will have repeatable sensing errors such as a constant offset, or bias. We have simulated the effect of an constant offset in the curvature sensor on the profile reconstruction uncertainty. This type of bias is expected for a curvature sensor based on an interferometer which may have a reference surface with residual surface power. The result of the simulation is shown in Fig. 6. The simulations emphasize that the calibration offset must be known to a high degree of accuracy, because its effect on the peak-to-valley error in the reconstructed profile increases rapidly with part size.

In general, higher order errors may occur in addition to sensor bias. The true curvature k of a surface at the measurement location is a function of the measured curvature value $\tilde{k}$:

$$k = f(\tilde{k}) \tag{3}$$

or

$$k = \alpha + \beta \cdot \tilde{k} + \gamma \cdot \tilde{k}^2 + \ldots, \tag{4}$$

when f is expressed as a power series in $\tilde{k}$. The purpose of the calibration of the curvature sensor is to find the constants $\alpha, \beta, \gamma \ldots$, which determine the calibration. In many cases a linear model may suffice, but a non-linear model may be needed if the sensor is used at the ends of its dynamic range. Because the profile is obtained from measured curvatures through double integration (Eq. 1), a biased curvature sensor will yield a quadratic error in the reconstructed profile and the peak-to-valley value of this error increases rapidly with part size. Depending on the curvature of the test part, first-order curvature sensor errors ($\beta \neq 1$), and higher-order errors, may result in higher-order errors in the reconstructed profile.

A calibration can be made in several ways. When the linear calibration model Eq. 4 is used, at least two reference surfaces with known curvatures within the dynamic range of the curvature sensor are needed to determine α and β. A set

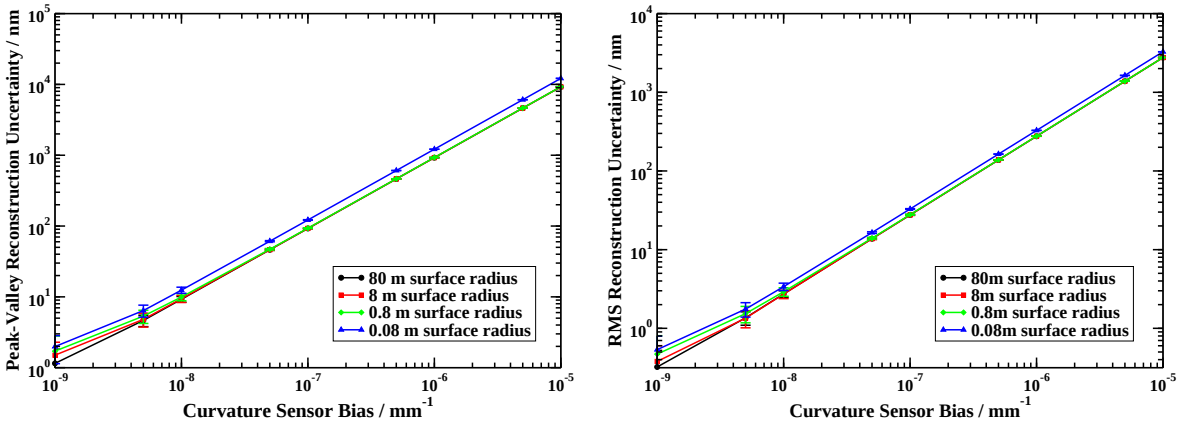

Figure 6. Profi le reconstruction uncertainty as function of curvature sensor offset, or bias, for surface radii of 0.08 m, 0.8 m, 8 m, and 80 m. A constant statistical standard uncertainty in the curvature sensing of 10^{-8} mm^{-1} is assumed.

of calibrated precision balls and spherical caps are suitable calibration artifacts which could be made to realize reference curvatures throughout the dynamic range of the sensor. An alternative method was described by Schulz et al.[9] who propose using a special diamond-turned aspheric surface, which must be characterized with an interferometer, for the calibration of the curvature sensor. In this method, the calibration model is adjusted until the reconstructed profile matches the known surface profile. A wide range of curvatures, which match the dynamic range of the curvature sensor, can be generated with relative ease.

4. MEASUREMENT OF AN ELLIPTICAL MIRROR

In section 3 we concluded that GEMM in its current form should be able to measure the profile of a mirror with a large radius using the 10 mm measurement objective of the instrument. We have put GEMM to the test and measured a profile of a mirror that has the form of an elliptical torus and was designed as part of a Kirkpatrick-Baez imaging system for an x-ray beam-line at the Advanced Photon Source (APS) of Argonne National Laboratory (ANL). A photo of this mirror is shown in Fig. 7. The mirror substrate is made from silicon; it is 90 mm long and 19 mm wide. The reflective surface of the mirror was polished into a sphere with radius of ≈84 m. A gold coating with varying thickness is deposited on the spherical surface to give the mirror an elliptical profile in the long direction. We measured a profile at the center of the mirror in the long direction with GEMM, with the Long Trace Profiler (LTP) at the APS, with the "eXtremely accurate CALIBration InterferometeR" (XCALIBIR) at NIST, and the Moore M48 coordinate measuring machine also at NIST. These instruments are described briefly in the sections below.

Proper calibration of the GEMM curvature sensor, as described in section 3.3, is difficult because suitable calibration artifacts with large radii, and curvatures within the dynamic range of the interferometer with 10 mm aperture, were not available. Because the range of curvatures on the elliptical x-ray mirror is small, we assume that $\beta = 1$ and neglect higher-order terms in Eq. 4. The offset α in Eq. 4 was determined using flatwith 50 mm diameter and a flatness error of $\lambda/40$ (at λ=633 nm). The curvature of this flat surface was measured at several random locations and the resulting curvature values were averaged which yielded a curvature offset α of 1.05×10^{-6} mm^{-1}.

An additional problem in comparing the profiles measured with different instruments arises, because each instrument used a different part coordinate system, each shifted by an unknown distance, to describe the profile. When comparing two profiles it is then necessary to shift one with respect to the other until the best possible agreement is achieved to compare measurements. When comparing two non-spherical profiles, $z_a(y)$ and $z_b(y)$, by shifting one with respect to the other until the difference in a least-squares sense is as small as possible, information about the parabolic component in the profile is potentially lost. We illustrate this fact by considering two third-order profiles

$$z_a(y) = a_0 + a_1 y + a_2 y^2 + a_3 y^3 \tag{5}$$

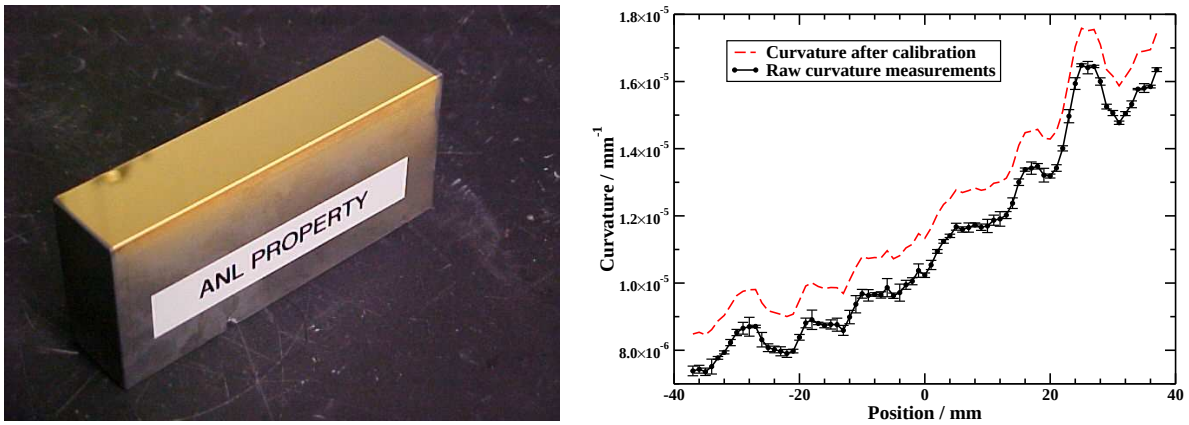

Figure 7. Elliptical torus designed as part of a Kirkpatrick-Baez imaging system for an x-ray beam-line (left). The GEMM measurement of the mirror curvature along the center line is shown on the right. The dashed line is the curvature after calibration by adding an offset α=1.05×10^{-6} mm^{-1}.

and

$$z_b(y-\delta y) = b_0 + b_1(y-\delta y) + b_2(y-\delta y)^2 + b_3(y-\delta y)^3. \tag{6}$$

Profile z_b is shifted by an amount δy with respect to z_a. The difference between the profiles is

$$\begin{aligned} z_b(y-\delta y) - z_a(y) \quad = \quad & y^3(b_3-a_3) \\ & +y^2(b_2-a_2-3b_3\delta y) \\ & +y(b_1-a_1+3b_3\delta y^2-2b_2\delta y) \\ & +b_0-a_0-b_1\delta y+b_2\delta y^2-b_3\delta y^3. \end{aligned} \tag{7}$$

When offset and slope (third and fourth term on the right-hand side of Eq. 7) are disregarded, the best match between profiles z_a and z_b is achieved when the shift, δy, is chosen such that

$$b_2 - a_2 = 3b_3\delta y, \tag{8}$$

and the second term on the right-hand side of Eq. 7 vanishes. All information about the difference in the second-order terms of the profiles is then lost from the best-fit profile difference. In general, a shift in a polynomial term of a certain degree results in errors in all polynomial terms with a lower degree. An error in the position of a third order polynomial adds errors in the second, first, and offset terms of the difference. A circular profile is approximately equal to a 2^{nd} order polynomial, and thus only causes an error in offset and slope, both of which are removed. An ellipse, however, yields approximately a parabolic profile difference which is similar to an error in the average radius of curvature. The resulting P-V and RMS errors are proportional to the shift in position.

The lesson is that for asymmetric profiles the relative position of the profiles needs to be known, as shifts result in errors of the lower order terms that cannot be distinguished from similar errors in the measurement instrument. In the case of our elliptical mirror, the result is a loss of information about the average radius of curvature.

4.1. The APS Long Trace Profiler

The long trace profiler (LTP) is a non-contact slope, or angle, measuring device that is widely used for measuring the surface figure of synchrotron beam-line mirrors. The original idea, credited to Takacs et al.,[16–18] was based on the pencil beam interferometer technique originally developed by von Bieren.[19] Variations of the original design are now in use worldwide.

The APS LPT II long trace profiler of the Advanced Photon Source (APS) (seen in Fig. 8 on the left) is the second generation of this instrument and was commissioned in 1994. The profiler has a number of improvements, including an

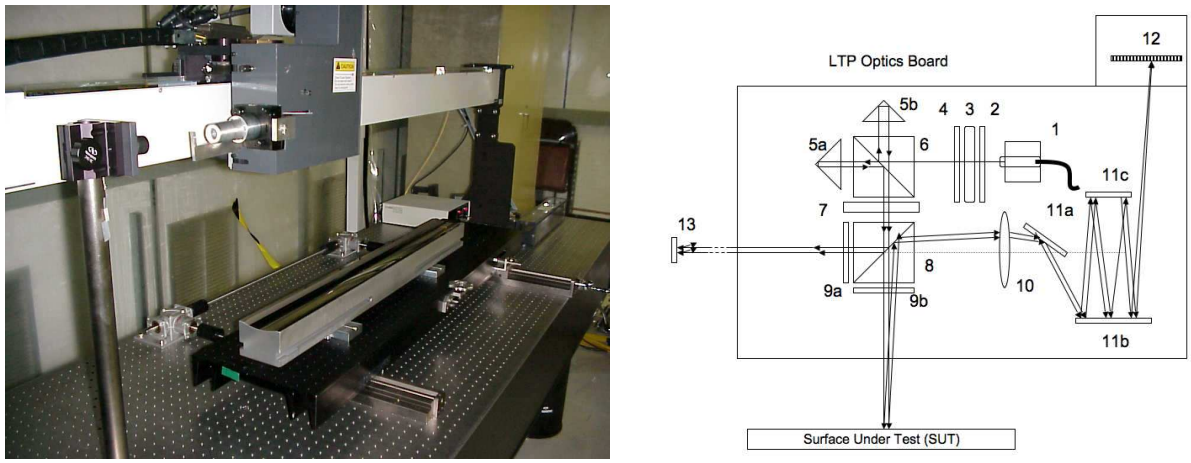

Figure 8. The Advanced Photon Source long trace profiler system APS LPT II, with a 1 m long cylindrical mirror set up for measurement (left). Optical schematics of LTP II (right). 1 = Laser fiber mount; 2 = Fixed polarizer; 3 = Rotating polarizer; 5a-b = Porro prism; 6 = Beam splitter; 7 = Rotating half-wave plate; 8 = Polarizing beam splitter; 9a-b = Quarter-wave plates; 10 = Fourier transform lens; 11a-c = Folding mirrors; 12 = 1024 pixel double array detector; 13 = Stationary reference mirror. Upon reflection from the Surface Under Test (SUT), the probe beam components are directed to the Fourier transform lens (10) by the polarizing beam splitter (8). The lens focuses the two beam components onto the linear array detector (12) and produces and intensity pattern with two peaks and a minimum between them. The location of the minimum is proportional to the measured local slope, and this minimum translates across the detector as the surface slope changes. In a similar fashion, the reference beam components detect the slope due to optics board pitch as it moves on the linear air bearing system. For clarity, the full path of the reflected components of the reference beam is not shown. At the end of a scan, the reference signal is subtracted from the SUT signal to obtain the true slope profile.

internally generated reference beam that is used to correct for tilt errors of the optical board, a dove prism (not shown in Fig. 8) that is incorporated into this reference beam to correct for phasing problems between the mechanical and thermal errors, and an environmental enclosure that stabilizes the temperature to within $\pm 0.1\,^{\circ}$C, which greatly improves instrument repeatability. Measurements performed on a 500 mm long Zerodur substrate show a standard uncertainty below 0.3 μrad rms, and a corresponding standard uncertainty for the height of 4.6 nm.[18] The angular range of the LPT is ± 5 mrad and it can handle mirrors up to 2 m long.

The mirror in Fig. 7 was set up on the APS LPT II table with the gold coated side facing up and was left for several hours to thermally stabilize. The mirror was first measured in one orientation. Then it was rotated by 180° about a vertical axis through the center of the mirror, and measured again. Ten scans were made at each orientation and the results were averaged to improve the signal-to-noise ratio. Additionally, at each of these orientations, the mirror was measured at three different tilt positions. In doing this, the beam probe takes different paths through both the polarizing beam splitter and the Fourier transform lens and averaging the resulting data reduced systematic uncertainties arising from these components. Finally, the data measured with the rotated mirror are rotated back numerically before averaging with data from the measurements with the unrotated mirror to arrive at the final tangential slope profile for the mirror.

4.2. Subaperture Stitching Interferometry with XCALIBIR

The mirror in Fig. 7 was measured with the "eXtremely accurate CALIBration InterferometeR" (XCALIBIR) at NIST. A solid model of the interferometer configuration is shown in Fig. 9. The XCALIBIR interferometer is built on a granite table to isolate it from seismic vibrations. The interferometer is housed in a class 1000 clean room that maintains the air temperature at $(20 \pm 0.02)\,^{\circ}$C to achieve the structural stability necessary for measurements such as radius-of-curvature measurements. Source and imaging components of the interferometer are set up on an elevated optical breadboard to create sufficient clearance for the testing of large parts. Light from the laser source is delivered to the interferometer with optical fibers. An off-axis parabolic mirror collimates the central part of the light cone that is emitted by the optical fiber and creates a collimated beam parallel to the top surface of the granite table. A beam splitter directs a fraction of the return beam from the part under test to the imaging arm of the interferometer and the camera. A beam expander, consisting

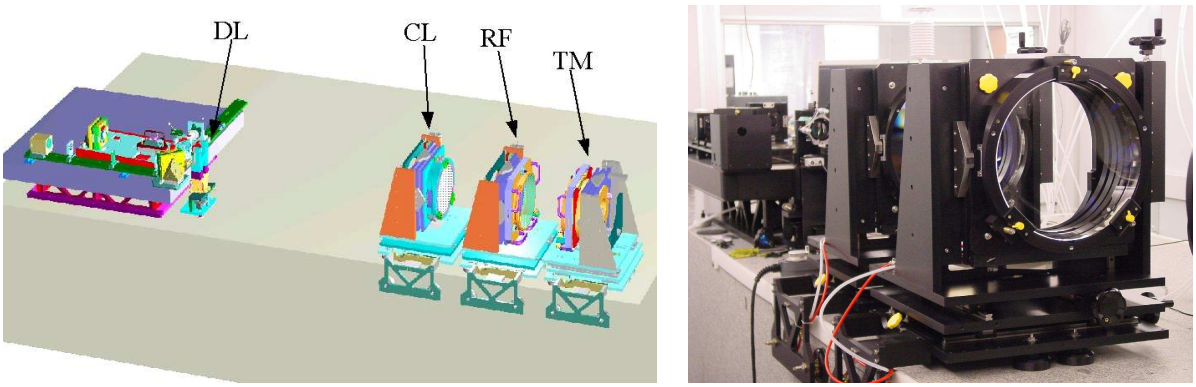

Figure 9. XCALIBIR interferometer configured for flatness measurements. The main components of the interferometer, from left to right, are: breadboard with source and imaging optics, diverger lens (DL), collimator lens (CL), reference flat (RF), and test mount (TM). The mirror in Fig. 7 was mounted on the test mount and the form error was measured by combining 5 sub-aperture measurements. A photo of the interferometer in its clean-room environment is shown on the right.

of an f/4 diverger lens and an f/4 collimator lens, creates a collimated test beam with just over 300 mm diameter. For the measurements of the gold-coated mirror surface described here, a reference flat with a Dynaflect† coating was used, which provided good fringe contrast for the highly reflective surface. Several measurements of the mirror with three or five sub-apertures were made. The subaperture measurements were then "stitched" together numerically.

4.3. The Moore M48 Coordinate Measuring Machine

The NIST M48 coordinate measuring machine, shown in Fig. 10, is widely regarded as the most accurate CMM of its size in the world. The machine structure consists of a heavy cast iron, jig-grinder base set on three vibration-damping mounts. The X-axis table and the Y-axis cross-carriage motions are carried out by high precision lead screws immersed in oil baths and are guided by precision double-"V" roller ways and assisted by constant force springs to reduce backlash to insignificant levels. The Z-axis motion is achieved through a counterweighted ceramic ram hung by another precision leadscrew and guided by air bearings and constant force springs. Laser interferometers are used on all three axes. A 200 mm thick, kinematically mounted granite surface plate on the machine table transforms complex table bending errors into more easily corrected rigid body motion errors. The machine is currently housed in a very stable laboratory environment. The humidity controlled room is maintained at a temperature of 20.00 °C ±0.01 °C. The local machine temperature environment is monitored through a series of 14 sensors placed in and around the machine for finer assessment of the thermal environment. The current probing system uses hydraulically damped and independent deformable parallelograms for all three axes of

Figure 10. Moore M48 coordinate measuring machine in the Advanced Metrology Laboratory at NIST.

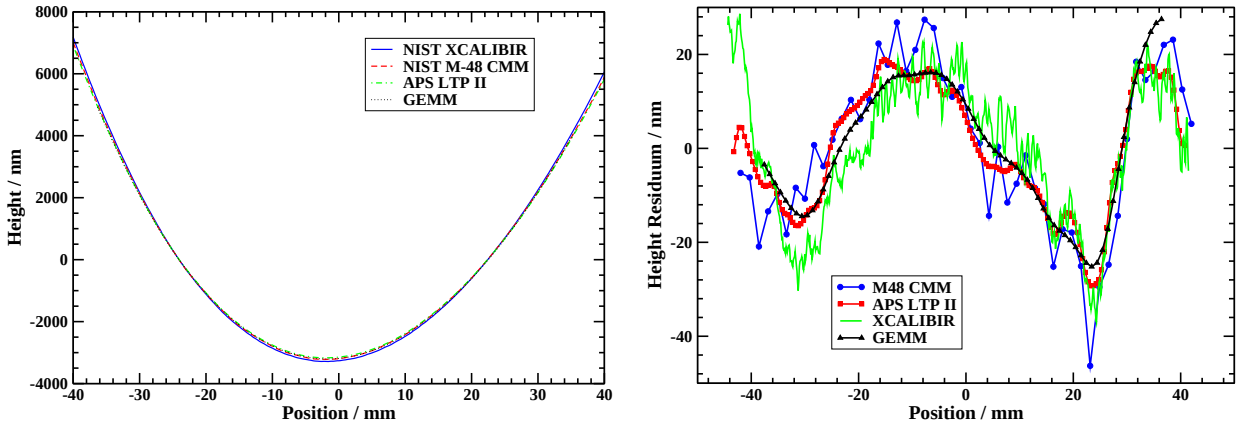

Figure 11. Profi les at the center of the mirror in Fig. 7 in the long direction, measured with the APS LTP II profi ler, the XCALIBIR interferometer at NIST, and the Moore M48 coordinate measuring machine at NIST. The graphs on the right show the GEMM, XCALIBIR, LTP, and CMM measurements with the nominal elliptical profi le of the mirror subtracted.

motion and provides repeatability at the level of 10 nm. Redundant error mapping and process control techniques have achieved a 2D positioning accuracy over an area of 600 mm $\times$ 600 mm of better than 50 nm for all optical and touch probe measurements.

4.4. Comparison of Profile Measurements

A comparison of the central profile of the mirror in Fig. 7, measured with the APS LTP II profiler, the XCALIBIR interferometer, the M48 CMM, and GEMM is shown in Fig. 11. The graph on the left of Fig. 11 shows all four profile measurements with offset and slope subtracted. The graph on the right of Fig. 11 shows the same data but with the elliptical profile of the mirror subtracted. The curvature data on which the reconstructed GEMM profile is based are shown in Fig. 7. The parameters of the nominal elliptical mirror profile were known and the nominal ellipse was oriented to match the profile measured with the M48 CMM. The elliptical profile was then subtracted from the CMM data. The residual profile is shown in Fig. 11 on the right. Using different instruments made it difficult to accurately relate the position coordinates of the different measurements. To compare the profiles, the GEMM, LTP, and XCALIBIR profiles were shifted, until the best possible agreement, in a least-squares sense, with the ellipse describing the nominal mirror profile was achieved. The ellipse was then subtracted; the residuals are shown in Fig. 11. As we have described above, the result of the profile shifts, which are necessary for the comparison, none of the profile errors shown in Fig. 11 contain information about the quadratic term of the profile error. All four profile errors agree to within 20 nm, which is not far from the expected profile reconstruction uncertainty for the curvature sensing uncertainty with the 10 mm GEMM objective (see Table 1 and Fig. 4).

5. CONCLUSION

Simulations of the profile reconstruction uncertainty for the Geometry Measuring Machine (GEMM) at NIST for the dominant measurement uncertainties have resulted in a set of requirements that must be met by any instrument of the GEMM type if it is to be used for measurements of precision optics where measurement uncertainties close to 1 nm are needed. While the necessary positioning accuracy of the curvature sensor is not difficult to meet for a wide range of surfaces, as long as the departure of the asphere from the best-fit sphere is modest, it is a considerably greater challenge to achieve the required curvature sensing uncertainty below $10^{-8}\,\mathrm{mm}^{-1}$. The compact Twyman-Green interferometer, which is currently used as curvature sensor in GEMM, comes close to this uncertainty with only one of its measurement objectives. Based on our experience with this interferometer, we estimate that we can achieve an uncertainty as low as $5{\cdot}10^{-9}\,\mathrm{mm}^{-1}$ with a new interferometer designed specifically for curvature sensing which is currently being constructed at NIST. The calibration curve (Eq. 4) must be known to a high degree of accuracy, in particular the offset α, because its effect on the peak-to-valley error in the reconstructed profile rises quadratically with profile length. Sensor stability is

equally important. For a profile of 86 mm length a stability better than $10^{-9}\,\mathrm{mm}^{-1}$ is needed for reconstruction errors of about 1 nm. Our profile measurement of an elliptical x-ray mirror with the GEMM prototype and with three other well-established metrology tools show, that the third- and higher-order profile error measurements from all instruments agree within 20 nm. Future work on GEMM will be directed towards developing a robust calibration procedure for the curvature sensor, and a new comparison of GEMM with other metrology tools in such a way that the important parabolic terms of profiles can be compared.

Acknowledgments

We are grateful to Dr. Robert S. Polvani for his support and help in making the GEMM project a success. The Argonne National Laboratory portion of this work was supported by the U.S. Department of Energy, Office of Basic Energy Sciences, under Contract No. W-31-109-ENG-38.

Disclaimer

†Certain commercial equipment, instruments, or materials are identified in this document. Such identification does not imply recommendation or endorsement by the National Institute of Standards and Technology, nor does it imply that the products are identified are necessarily the best available for the purpose.

REFERENCES

1. M. P. do Carmo, *Differential Geometry of Curves and Surfaces*, Prentice Hall, 1976.
2. J. J. Stoker, *Differential Geometry*, Wiley-Interscience, New York, 1969.
3. P. E. Glenn, "Angstrom level profilometry for submillimeter- to meter- scale surface errors," in *Advanced Optical Manufacturing and Testing*, G. M. Sanger, P. B. Reid, and L. R. Baker, eds., *Proc. SPIE* **1333**, pp. 326–336, 1990.
4. P. E. Glenn, "Lambda-over-one-thousand metrology results for steep aspheres using a curvature profiling technique," in *Advanced Optical Manufacturing and Testing II*, V. J. D. D.V.M, ed., *Proc. SPIE* **1531**, pp. 64–61, 1992.
5. I. Weingärtner, M. Schulz, and C. Elster, "Novel scanning technique for ultra-precise measurement of topography," in *Optical Manufacturing and Testing III, Proc. SPIE* **3782**, pp. 306–317, 1999.
6. I. Weingärtner, M. Schulz, P. Thomsen-Schmidt, and C. Elster, "Measurement of steep aspheres: a step forward to nanometer accuracy," in *Optical Metrology for the Semiconductor, Optical, and Data Storage Industries II*, A. Duparré and B. Singh, eds., *Proc. SPIE* **4449**, pp. 195–204, 2001.
7. I. Weingärtner, M. Schulz, R. D. Geckler, O. Jusko, M. Neugebauer, A. Nicolaus, and G. Bönsch in *Recent Developments in Traceable Dimensional Measurements*, J. E. Decker and N. Brown, eds., *Proc. SPIE* **4401**, pp. 175–183, 2001.
8. M. Schulz, "Topography measurement by a reliable large-area curvature sensor," *Optik* **112**, pp. 86–90, 2001.
9. M. Schulz and I. Weingärtner, "Measurement of steep aspheres by curvature scanning: an uncertainty budget," *Proc. of 2*$^{\mathrm{nd}}$ *euspen International Conference* , pp. 478–481, 2001.
10. I. Weingärtner, M. Schulz, C. Elster, J. Gerhardt, and A. Lucas, "Simultaneous distance, slope, curvature, and shape measurement with a multi-purpose interferometer," in *Interferometry IX*, W. Osten, ed., *Proc. SPIE* **4778**, pp. 198–205, 2002.
11. C. Elster, J. Gerhardt, P. Thomsen-Schmidt, M. Schulz, and I. Weingärtner, "Reconstructing surface profiles from curvature measurements," *Optik* **113**, pp. 154–158, 2002.
12. M. Schulz, I. Weingärtner, C. Elster, and J. Gerhardt, "Low- and mid-spatial frequency components measurement for aspheres," in *Advanced Characterization Techniques for Optics, Semiconductors, and Nanotechnologies*, A. Duparrë and B. Singh, eds., *Proc. SPIE* **5188**, pp. 287–295, 2003.
13. M. Schulz, R. D. Geckeler, and J. Illemann, "High accuracy form measurement of large optical surfaces," in *Recent developments in traceable dimensional measurements II*, J. E. Decker and N. Brown, eds., *Proc. SPIE* **5190**, pp. 211–219, 2003.
14. C. Wagner and G. Häusler, "Information theoretical optimization for optical range sensors," *Appl. Opt.* **42**, pp. 5418–5426, 2003.

15. C. Elster and I. Weingärtner, "High-accuracy reconstruction of a function $f(x)$ when only $\frac{d}{dx}f(x)$ or $\frac{d^2}{dx^2}f(x)$ is known at discrete measurement points," in *X-ray Mirrors, Crystals, and Multilayers II*, A. K. Freund, A. T. Macrander, T. Ishikawa, and J. L. Wood, eds., *Proc. SPIE* **4782**, pp. 12–20, 2002.
16. P. Z. Takacs and S. N. Qian, "Design of a long trace surface profiler," in *Metrology: Figure and Finish*, B. E. Truax, ed., *Proc. SPIE* **749**, pp. 59–64, 1987.
17. P. Z. Takacs and S. N. Qian, "Surface profile interferometer. U.S. Patent 4,884,697," 1989.
18. P. Z. Takacs, E. L. Church, C. Bresloff, and L. Assoufid, "Long trace profiler measurement repeatability improvements," *Appl. Opt.* **38**, pp. 5468–5479, 1999.
19. K. von Bieren, "Pencil beam interferometer for aspherical optical surfaces laser diagnostics," *Proc. SPIE* **343**, pp. 101–108, 1982.